Fibers and Polymers 2009, Vol.10, No.5, 716-723 DOI 10.1007/s12221-010-0716-2

Homogeneous Self-cleaning Coatings on Cellulose Materials Derived from TIP/TiO_2 P25

Nika Vero*, Silvo Hribernik, Patrizia Andreozzi[1], and Majda Sfiligoj-Smole

Characterization and Processing of Polymers Laboratory, University of Maribor, Smetanova 17, Slovenia
[1]Department of Chemistry, Sapienza University, I-00185 Rome, Italy
(Received February 27, 2009; Revised June 30, 2009; Accepted July 13, 2009)

Abstract: The aim of this research was to study TiO_2 nanocoatings formation and to investigate their self-cleaning effects when applied on cellulose materials. Two different approaches for achieving nanocoatings were used. First, coatings were generated in situ through an acid and alkaline catalyzed sol-gel process with or without added water. Another type of coatings was prepared starting from commercial TiO_2 P25 powder. In order to acquire homogeneous coatings from TiO_2 P25 nanoparticles with uniform nanoparticles size distribution, pH of aqueous TiO_2 P25 dispersions was varied. The dispersion preparation conditions were studied by dynamic light scattering (DLS) and zeta potential (ζ-potential) analysis. The resulting TiO_2 nanocoatings were analyzed in terms of their surface morphology using scanning electron microscopy (SEM). Nanocoatings obtained from pure aqueous dispersions of TiO_2 P25 nanoparticles were inhomogeneous with huge agglomerates; however by changing the pH of dispersion and consequently changing the surface charge of TiO_2 P25 nanoparticles as well, more homogeneous nanocoatings with uniform TiO_2 nanoparticles distribution were prepared. Significant differences between sol-gel derived coatings were observed. Sol-gel process without added water yielded more homogeneous coatings than sol-gel process with addition of water. Completely different surface morphologies were obtained using alkaline or acid catalyst. Acid catalyzed sol-gel process yielded nanocoatings with long, extended, thin structures; contrary, under alkaline conditions particles grow in size with decrease in number. Fourier transform infrared (FTIR) spectroscopy was used to study the coatings' microstructure. Furthermore the formation of mono-disperse nanoparticles on the fiber surface resulted in enhanced photocatalytic activity. Degradation of colored stain applied on TiO_2-treated samples was investigated by colorimetric measurements. Photocatalytic activity of nanocoatings prepared via acid catalyzed sol-gel process without water addition was comparable to that of nanocoatings derived from aqueous dispersions of commercial TiO_2 P25 nanoparticles.

Keywords: Self-cleaning, TiO_2 coating, Sol-gel process, ζ-potential, DLS, FT-IR

Introduction

Nano titanium dioxide (TiO_2) is a promising material with broad applications in coating technologies (e.g. for indoor as well as outdoor applications, providing easy-to-clean, anti-adhesive and potentially also antimicrobial surfaces based on photocatalysis). Numerous techniques for production of nanocoatings exist, such as sol-gel coating process and coating process using pre-formed nanoparticles.

The preparation and properties of xerogels have been comprehensively studied [1-10]. These materials are prepared through sol-gel processing, in which precursor solutions undergo gelation, aging and drying. Liquid-vapor interfaces develop in the drying gel, and forces due to surface tension cause substantial collapse of the gel structure as liquid is removed [11,12]. The H_2O:Ti molar ratio (R) is a ratio between water and precursor and plays a major part in the structure development process of sol-gel materials. Sol particle size and cross-linking inside the particles (density) is pH and R-value dependant [11]. By controlling the synthesis conditions carefully, these reactions may lead to a variety of structures, and to different final states of the material [13,14]. Typical precursors for TiO_2 synthesis are titanium chloride, sulfate and alkoxides. As alkoxide precursor titanium isopropoxide, ethoxide and butoxide are used [15-24]. Much work has been carried out depositing TiO_2 on heat resistant surfaces like glass, ceramics and silica by sol-gel methods, where temperatures up to 500 °C can be used. Some reports on TiO_2 application in on textile can be found as well [25-27].

In addition to, nanocoatings are prepared by using pre-formed nanoparticles. TiO_2 P25, a commercial TiO_2 photocatalyst produced by Degussa containing a mixture of rutile and anatase crystalline forms, has proven to be the best photocatalyst towards a broad range of organic pollutants [28-32]. TiO_2 powders consist of primary particles, agglomerates and aggregates [33]. However, they only present the best properties in the systems where they are used, if they are optimally separated into smaller size populations. Therefore the dispersing process of TiO_2 powder is a critical step in the production of coated materials. In colloid aqueous dispersions of TiO_2 nanoparticles, the particles rapidly agglomerate, which results in reduction of the effective photocatalytical activity of surface. Controlling the agglomeration of nanoparticles by reducing van der Waals and enhancing repulsive Colomb interactions, would considerably increase the applicability of TiO_2 nanoparticles dispersions. Pure TiO_2 has its isoelectric point (IEP) at pH-values in between 4.5 and 6.5 [33,34]. In aqueous systems, the IEP of TiO_2 considerably influences

*Corresponding author: nikaveronovski@gmail.com

the flocculation behavior, thus TiO_2 aqueous dispersions can be stabilized merely by adjusting the pH-value [33].

In the paper two kinds of coating processes were studied in detail. The aim of research was to obtain highly photocatalytically active nanocoated fibers, therefore homogeneous coatings with narrow distribution of particles' sizes by in situ approach through sol-gel process; and by adsorption of TiO_2 P25 nanoparticles were prepared. To study the impact of the coating conditions on formation of coating with uniform particle size distribution of high functionality different techniques were used, e.g. DLS and ζ-potential analysis. To verify the efficiency of the coating process, surface morphology, microstructure and self-cleaning properties of generated nanocoatings were investigated using SEM, FTIR analysis and colorimetric measurements.

Experimental

Material and Samples Preparation

Two different methods for TiO_2 coatings procedure were used; the sol-gel process and adsorption of pre-formed TiO_2 nanoparticles.

Sol-gel Procedure for Nanocoatings Preparation

Materials: In the sol-gel process for preparation of nanocoatings, the following chemicals were used as received: the precursor Titanium isopropoxide, TIP 97 % (Aldrich, Germany), Ethanol, 99 % (Merck, Germany), Isopropanol, 99 % (Aldrich, Germany), acetic acid, 100 % (Merck, Germany), ammonia solution, 25 % (Merck, Germany) and deionized water were used. Regenerated cellulose Lyocell fibers (Fineness 1.17 dtex) and fabric in 2/1 twill weave with S twill line (Weight per unit area: 155.63 cm^{-2}; Warp: 40 yarns cm^{-1}; Weft: 30 yarns cm^{-1}), (Lenzing, Austria) were used as a base material.

Coating process: In order to modify cellulose surfaces with TiO_2 nanoparticles, sol-gel coating process with addition of water was applied under different pH conditions; acid (TIPAq-A) and alkaline (TIPAq-B). Titanium (IV) isopropoxide (TIP) was used as precursor and two catalysts (acetic acid or ammonia solution) were used for the synthesis. After mixing a 0.5 mol l^{-1} TIP with isopropanol, fibers were added. A 0.5 mol l^{-1} NH_3 or a 0.5 mol l^{-1} CH_3COOH in 6 mol l^{-1} deionized water was added to the reaction mixture. The whole mixture was kept at 50 °C for 1 h under vigorous stirring. Upon this time, the samples were dried overnight at room temperature, and then thermally treated at 110 °C for 15 min.

In the sol-gel coating process without added water TiO_2 particles were synthesized directly onto the fabric, just like in the former coating process. The fabrics were soaked in an acetic acid (TIP-A; 10 m*l* of 100 % acetic acid in 40 m*l* isopropanol) or ammonia solution (TIP-B; 10 m*l* of 25 % ammonia solution in 40 m*l* isopropanol) for approximately 1 h before placing them in between two filter papers soaked in solution of TIP (10 vol% in isopropanol). To allow the reagents to be homogeneously absorbed, the fabrics were carefully blotted and left for 4 h in a covered Petri dish. After that, the fabric was immersed in pure isopropanol for at least 1 day in order to remove any free unattached titanium particles. The fabric was dried at room temperature and thermally treated for 2 h at 80 °C.

Adsorption of TiO_2 P25 Nanoparticles on Cellulose Fibers

Materials: In order to modify the surface of regenerated cellulose Lyocell fibers/fabric, commercial TiO_2 nanoparticles (TiO_2 P25, Degussa, Germany) were used. According to the manufacturer, the main properties of the nanoparticles are: (i) surface area: (50±15) m^2 g l^{-1}, (ii) size: 21 nm, (iii) density: 4 g cm^{-3}. For adjusting the pH value of dispersions, 0.1 M HCl and 25 % ammonia solution were used, respectively.

Dispersions Preparation: Initially, aqueous 5 mg ml^{-1} TiO_2 P25 nanoparticles dispersion (P25Aq) was pre-dispersed in an ultrasound bath Elma with the frequency of 35 kHz at 40 °C for 30 min. In addition, acid (P25Aq-A) and alkaline (P25Aq-B) dispersions were prepared. For preparation of P25Aq-A dispersion, pH-value was adjusted with 0.1 M HCl and for preparation of P25Aq-B dispersion, 25 % ammonia solution was used.

Coating Process: Preparation of dispersions was followed by coating of fibers/fabrics. 5 mg ml^{-1} TiO_2 P25 dispersions were used. 0.5 g of sample was immersed into the P25Aq, P25Aq-A and P25Aq-B dispersion, respectively, and treated at room temperature during the night. Treated samples were air dried.

Designations of differently coated samples are collected in Table 1.

Analytical Techniques

Characterization of TiO_2 P25 Dispersions

Zeta Potential (ζ-potential) Analysis: A Malvern laser-velocimetry Doppler utility (Zetasizer Nano series HT, Malvern UK) was used for ζ-potential analysis [35,36]. The electro-phoretic mobility data, μ (m^2 sV^{-1}), of the dispersions were transformed into ζ-potential according to [37]

Table 1. Samples designation

Sample	Designation
TIPAq-A	Acid catalyzed sol-gel coating process with addition of water
TIPAq-B	Alkaline catalyzed sol-gel coating process with addition of water
TIP-A	Acid catalyzed sol-gel coating process without added water
TIP-B	Alkaline catalyzed sol-gel coating process without added water
P25Aq	Aqueous 5 mg ml^{-1} TiO_2 P25 nanoparticles dispersion (pH 6.3)
P25Aq-A	Acid 5 mg ml^{-1} TiO_2 P25 nanoparticles dispersion (pH 3.0)
P25Aq-B	Alkaline 5 mg ml^{-1} TiO_2 P25 nanoparticles dispersion (pH 10.0)

$$\zeta = \left[\frac{4\pi\eta\mu}{\varepsilon}\right] \quad (1)$$

where ε is a dielectric constant of the dispersing medium and η the solvent viscosity. Reproducibility of ζ-potential measurements of TiO_2 P25 dispersions was determined by calculations of variation coefficient (CV) for the ζ-potential. Very good repeatability was attained as the CV for ζ-potential was about 4 %.

Dynamic Light Scattering (DLS) Analysis: DLS analyses were performed using a Malvern light scattering unit, Zetasizer Nano series HT (Malvern, UK) [38]. DLS is a technique used to measure the Brownian motion (diffusion) and subsequent size distribution of an ensemble collection of particles in dispersion. Individual peaks in particle size distributions were derived from multi-modal correlation functions and fitting the data by CONTIN algorithms.

Characterization of Coated Materials

Scanning Electron Microscopy (SEM): Surface morphologies of coated fibers were studied by scanning electron microscopy (SEM, ZEISS Gemini Supra 35 VP), with a maximum resolution up to 5 nm. Fibers were fixed by adhesive carbon band on brass holders.

Fourier Transform Infrared (FTIR) Spectroscopy: The FTIR spectra of modified and unmodified fibers were obtained on a PerkinElmer FT-IR System Spectrum GX. The spectra of studied samples were recorded over the range 4000-600 cm^{-1} in absorbance mode.

Self-cleaning Test: Photocatalytic properties of coatings were investigated by determining stain discoloration, caused by the oxidation of the stubborn red wine stain. With the aim of studying the self-cleaning efficiency under real conditions, the self-cleaning test was not performed in an UV chamber as usually, but under conditions of direct daylight irradiation and after different periods of time. The intensity of the discoloration of the wine stain applied on the fabric surface due to the daylight irradiation was colorimetrically followed. UV index during the exposure under bright weather conditions was up to 8 [39]. Datacolor international MICROFLASH 200d apparatus was used for colorimetric measurements. Chroma (C^*) component of CIELAB color system was determined by a standard method [40,41].

Results and Discussion

Electrophoretic Mobility and Particle Size Distribution of TiO_2 P25 Nanoparticles

ζ-potential quantifies the conditions leading to the stability of TiO_2 P25 dispersions. It is a function of the surface charge density, and as such, any change in the surface charge will lead to changes in the measured ζ-potential. If the ζ-potential is > 30 mV or < −30 mV, the particles tend to repel each other, which increase the subsequent dispersion stability [42]. As the ζ-potential moves toward 0 mV (the isoelectric point) the possibility of particle aggregation increases, leading to a reduction in the stability. ζ-potential is always measured under dilute conditions and is strongly dependant on pH and additive concentrations. ζ-potential distribution shown on Figure 1 indicates instability of P25Aq dispersion (ζ-potential =12.6 mV) due to amphoteric character of TiO_2 nanoparticles. The IEP of the particles was found at pH~4.5. This value is comparable to that obtained for TiO_2 particles by other authors [33,34]. To improve dispersion stability the effect of dispersion pH was studied. Increasing and decreasing the pH value of dispersion increase the stability of TiO_2 P25 dispersions. In acid or alkaline environment the surface of TiO_2 P25 nanoparticles became charged. In addition to changes in the surface charge and charge density, the presence of acid or base modifies the double layer thickness around TiO_2 P25 particles. In such conditions the particles repel each other, which results in significant dispersion stability. The highest stability was observed for P25Aq-A dispersion, with ζ-potential of 35.2 mV. Addition of acid to aqueous P25Aq dispersion shifted pH sufficiently far away from the pH_{iep} gaining higher level of dispersability. ζ-potential of P25Aq-B dispersion was -33.3 mV due to the negative charge of TiO_2.

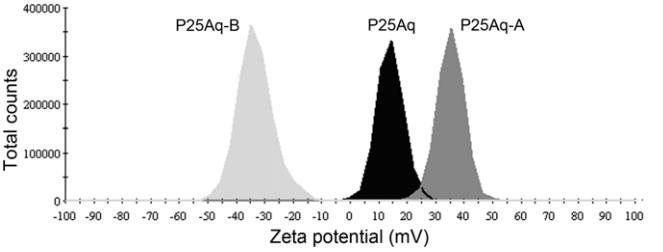

Figure 1. Distribution of ζ-potentials for TiO_2 P25 particles in aqueous dispersion (P25Aq), in acid dispersion (P25Aq-A) and in alkaline dispersion (P25Aq-B).

DLS measurements were carried out to determine the

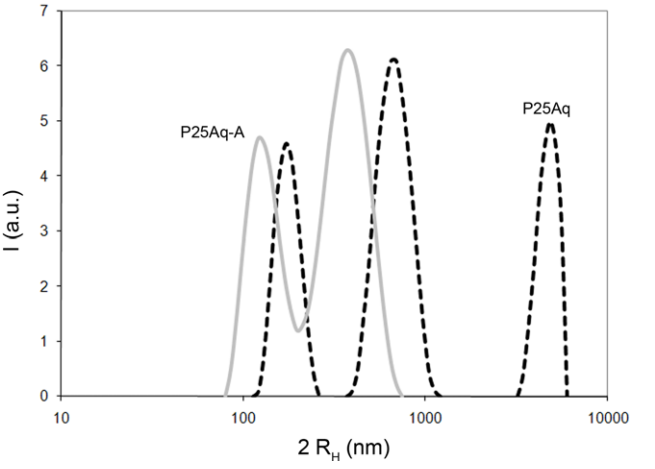

Figure 2. Size distribution plots of P25Aq (interrupted curve) and P25Aq-A dispersions (solid curve).

Table 2. The mean particle sizes of different P25 dispersions at each peak

Sample	Peak 1(nm)	Peak 2 (nm)	Peak 3 (nm)
pH 3.0	131.7	375.7	/
pH 6.3	175.1	675.8	4964
pH 10.0	/	881.8	5596

particle size distribution of TiO_2 P25 nanoparticles dispersions. Size distribution plot for P25Aq and P25Aq-A dispersions is presented at Figure 2. According to the plots in Figures 2 and 3, the samples contain different scattering populations; the first, fast moving populations, at 131-175 nm; the second at 375-882 nm; and the third, slow moving agglomerates, at 4964-5596 nm. Table 2 indicates the mean particle sizes of different P25 dispersions at each peak. As a result of pH adjustment to value 3.0 (P25Aq-A), we can observe a decrease in agglomeration tendency in comparison with P25Aq, only two smaller size populations occur, however the third peak is observed only for P25Aq dispersion. It indicates the occurrence of large agglomerates in P25Aq dispersion, and we can conclude that at lower pH values huge agglomerates are not formed.

At pH 10.0, the size distribution plot shows the presence of larger-size populations (Figure 3). Such conditions are not applicable in producing photocatalytically active surfaces. According to Chen *et al.* [43] the surface charge density on the particle surface no longer increases as pH increases to a high pH range since the ionization of the particle surface has reached saturation, but the double electrical layers around the particles are depressed, eventually resulting in decrease of dispersion stability.

Our results are in agreement with results reported by Regitsky, who found acidic conditions to be better for TiO_2 nanoparticles dispersion comparing to alkaline conditions [44].

The particle size distribution is of great importance because it affects photocatalytic activity of coated surfaces.

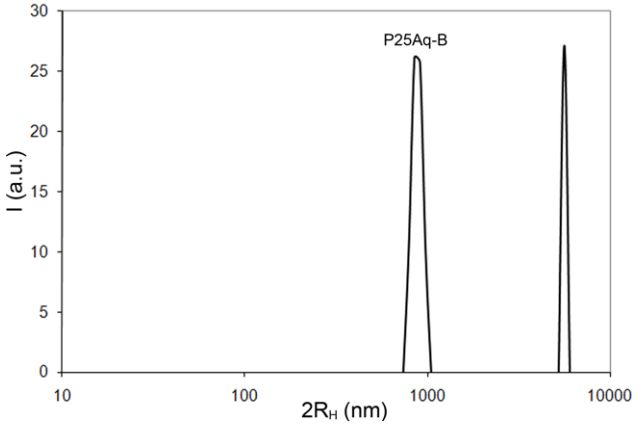

Figure 3. Size distribution plot of P25Aq-B dispersion.

Fibers Surface Observations

Fibers surface morphology before and after coating with TiO_2 was investigated on SEM images. The surface of untreated Lyocell fiber is smooth and without any particularity (Figure 4(A)). TiO_2-modifications change fibers' surface.

Figure 4(B) and 4(C) show the surface morphology of the fibers nanocoated via TIPAq-A and TIPAq-B sol-gel process. TIPAq-A process forms a coating, which doesn't coat the fiber surface entirely (Figure 4(B)). On the Figure 4(C) cracks are formed on the entire surface but we can already observe the formation of a defined structure. Incomplete formation of the coatings by the sol-gel processes with addition of water can be explained based on the fact that hydrolysis with addition of water is rapid and completed within seconds, due to the quick reaction between titanium isopropoxide and water upon contact.

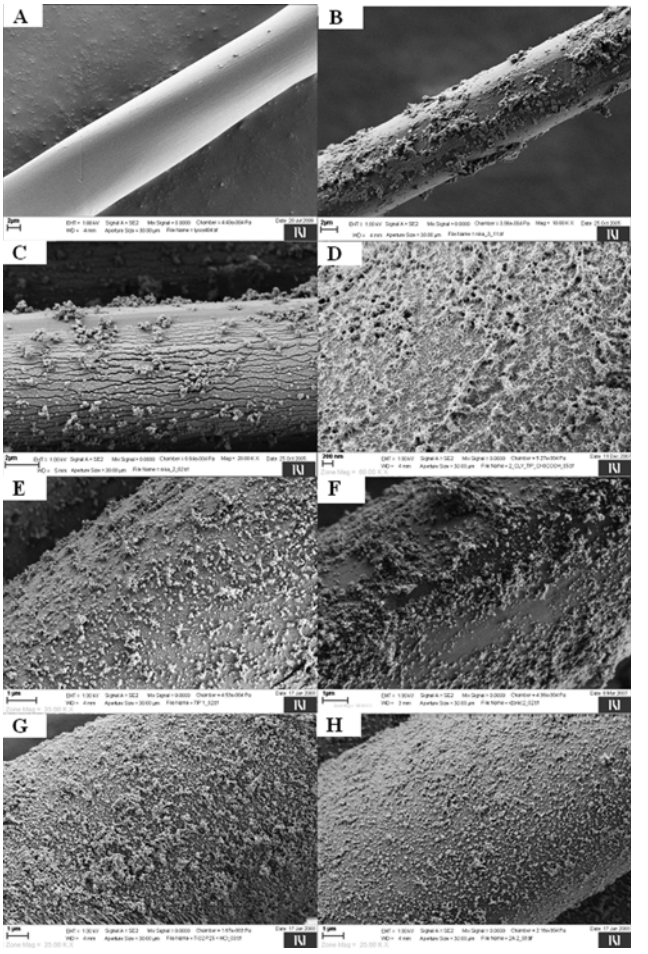

Figure 4. (A) SEM image of surface morphology of untreated Lyocell fiber; taken at magnifications of 10×10^3, (B) SEM images of surface morphologies of fibers treated via TIPAq-A, (C) TIPAq-B, (D) TIP-A, and (E) TIP-B sol-gel process; taken at magnifications of 10, 20, 60 and 35×10^3, respectively; SEM images of surface morphologies of fibers treated in (F) P25Aq, (G) P25Aq-A, and (H) P25Aq-B dispersion; taken at magnification of 25×10^3.

High reactivity was moderated by using sol-gel process without addition of water. Completely different surface morphologies were obtained using the same precursor and catalysts, only without added water, under conditions of slow hydrolysis (Figure 4(D) and 4(E)). For reaction of hydrolysis, moisture present in air was sufficient for it to proceed. A titanium network without agglomeration was formed in TIP-A process, which yielded nanocoatings with long, extended, thin structures (Figure 4(D)). That kind of coatings have large active surface, which plays an important role in the reactions of photocatalysis. Contrary, under alkaline conditions particles grow in size with decrease in number, since in the alkaline-catalyzed process a reaction of hydrolysis is slow and a reaction of condensation is rapid. Coatings with homogeneous distribution of spherical TiO_2 nanoparticles can be seen in Figure 4(E).

The obtained results are in agreement with previous reports about TiO_2 nanoparticles preparation [9,45]; however we succeeded in preparation of TiO_2 nanoparticles with a narrow distribution of sizes directly on the surface of fibers.

The results of DLS and ζ-potential measurements were verified by surface morphology analysis of yielded coatings. Coatings generated from unstable P25Aq dispersion, which contained big agglomerates, are irregular and big agglomerates can be seen on the fiber surface (see Figure 4(F)). Use of stable dispersions where the aggregation of fine particles into larger units was controlled with adjustment of pH value, yielded nanocoatings with uniform nanoparticles distribution (see Figure 4(G) and 4(H)).

FTIR Analysis of Untreated and Treated Lyocell Fibers

In order to determine structural changes of modified Lyocell samples and to foresee the binding mechanism of TiO_2 particles on cellulose fibers, the FTIR analysis was performed.

The FTIR spectra of unmodified and modified samples are shown in Figure 5 and 6. In the figures we can see the spectrum of raw cellulose fibers with many free hydroxyl groups on the surface, with characteristic bands at 3500-

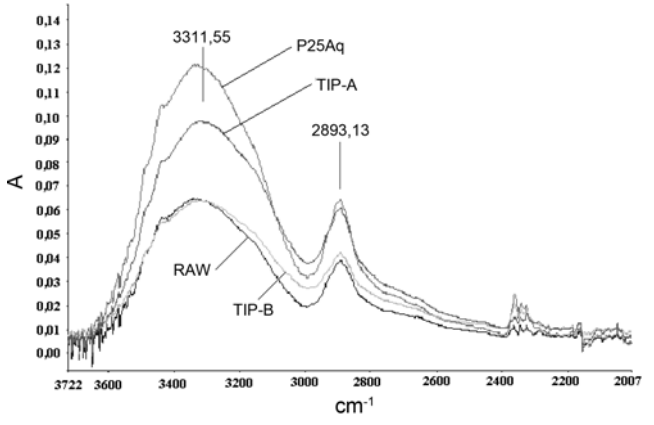

Figure 5. IR spectra of raw, TIP-A, TIP-B and P25Aq-treated fibres over the range 3600-2400 cm^{-1}.

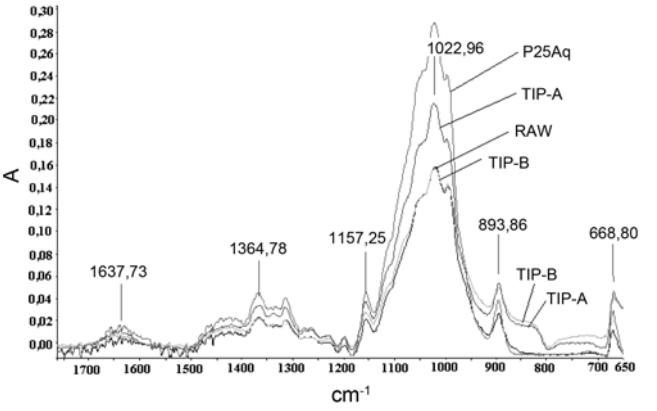

Figure 6. IR spectra of raw, TIP-A, TIP-B and P25Aq-treated fibres over the range 1500-600 cm^{-1}.

3200 cm^{-1}, due to O-H valent vibration of water, 2980-2800 cm^{-1}, due to C-H stretching, ~1640 cm^{-1}, due to deformation vibration of water molecules and absorption bands in the 1500-800 cm^{-1} spectral region, which occurred as a result of C-H, O-H, C-O and C-O-C vibration in glucosidic ring and represents the finger print of cellulose. Our results are in agreement with Tomšič *et al.* [46].

In Figure 5 and 6 we can observe the presence of TiO_2 on the surface of treated fibres, which can be seen as an increase in the intensity of absorption bands at 3311 cm^{-1} and 1023 cm^{-1} in the case of TIP-A and P25Aq treatment, due to interactions between hydroxyl groups of cellulose with hydroxyl groups of TiO_2. The intensity of absorption bands is lower in the case of TIP-B treated fibres. The interactions between hydroxyl groups of cellulose and surface hydroxyl groups of TiO_2 are described in more detail in the literature [47-49].

According to Parfitt the chemistry of the oxide surface is, to a large extent, dominated by the hydroxyl groups, which arises from the interaction of water or water vapor with the surface planes to achieve valency saturation [50]. Such groups act as active sites, which interact with the components of the surrounding medium [50-52]. Two different types of hydroxyl groups exists; one of these is associated with a metal site having monodentate attachment (terminal OH) and the other one an oxide site with bidentate attachment (bridged OH) [50]. The pure TiO_2 P25 specimen has ν(OH) stretching bands in the region between 3600 and 3000 cm^{-1} [53]. The intensity of the band at 3300 cm^{-1} has been attributed to a bridging hydroxyl groups. These results are in agreement with findings of Erdem *et al.* [53]. A broad band between 3500 and 3100 cm^{-1} corresponds to the O-H stretching mode of Ti-OH. Bands for Ti-O and Ti (O-C) vibrations are located at around 970 and 1080 cm^{-1}, respectively. An O-H bending vibration was observed at 1638 cm^{-1}. According to Sayilkan *et al.* the groups of Ti-O and Ti-O-C can form a connected network between TiO_2 particles [54]. The peak at 668 cm^{-1} refers to symmetric O-

Ti-O stretch while 505 cm^{-1} is due to the vibration of Ti-O bond. These findings are in accordance with Nur [55].

Absorption bands of untreated cellulose fibers and TiO_2-treated fibers in the 3722-2007 cm^{-1} and 1762-650 cm^{-1} spectral region at 3311, 2893 and 1023 cm^{-1} are overlapping, but differences can be observed, indicating the presence of TiO_2 particles on the surfaces of fibers. Based on results of surface morphology analysis, differences between IR spectra of TIP-A and TIP-B treated fibers are presumably due to different structure of yielded coatings.

Self-cleaning Efficiency

Since visual subjective color determination can lead to many misunderstandings, objective measurements were performed to determine the self-cleaning properties. For determination of self-cleaning activity we used only samples with homogeneous coatings and with uniform particles size distribution; selection was made on the basis of results of DLS and ζ-potential analyses and on the basis of SEM images. We used sample treated by TIP-A sol-gel coating process; sample treated by TIP-B sol-gel coating process; sample treated with P25-A dispersion and sample treated with P25-B dispersion. After the exposure of stained samples to daylight, we observed color changes of the stain. The more effectively titanium breaks down the organic dye the greater is impact on the stain color changes. Colorimetric measurements of CIELAB differences were performed during and after the test. TiO_2 modification caused color changes, because oxidative reactions resulted in the bleaching of the dye. Determination of color differences obtained by chroma (C^*) measurements was performed. The highest difference in C^* (ΔC^*) between unstained and stained samples means the best photocatalytic activity. All treated samples were stained in the same way; one drop of red wine was applied on the sample surface. After 1 h of daylight-exposure, C^* was measured. Changes in C^* between different samples were significant. After 42 days of daylight-exposure, measurements of C^* were repeated; reduction in C^* values was observed. We have calculated ΔC^* from $C_1{}^*$ and $C_{42}{}^*$. Chroma values of stain on modified fabrics after 1 day ($C_1{}^*$) and 42 days ($C_{42}{}^*$) of exposure to daylight and calculated differences of Chroma values (ΔC^*) are collected in Table 3. The best photocatalytic activity was determined for sample, coated with a P25Aq-A dispersion and daylight-irradiated for 42 days (ΔC^*=9.2), where the best photocatalytic degradation of organic compound (wine stain) was observed (71.37 %). Sample, coated with P25Aq-B dispersion followed (ΔC^*=8.58). Insignificantly lower photocatalytic activity was observed for photocatalytic activity of sample, coated via TIP-A process (ΔC^*=7.07). The lowest photocatalytic activity was observed for sample, coated via TIP-B process (ΔC^*=5.15).

Table 3. Chroma of stain on untreated (raw) and modified fabrics after 1 day ($C_1{}^*$) and after 42 days ($C_{42}{}^*$) of daylight-exposure and chroma differences ΔC^*

Sample	$C_1{}^*$	$C_{42}{}^*$	ΔC^*
Raw	14.23	10.42	3.81
1 TIP-A	17.31	10.24	7.07
2 TIP-B	12.02	6.87	5.15
3 P25-AqA	12.89	3.69	9.2
4 P25-AqB	13.52	4.94	8.58

The efficiency of photocatalytic activity was related to surface morphology of coating on fibers. In the case of sol-gel derived coatings, the best photocatalytic activity was observed for the coatings with full coverage, even thickness of uniform distribution of particle sizes; and in the case of dispersion-derived coatings, the best photocatalytic activity was observed for coatings with uniform particle distribution. In addition, the photocatalytic activity is strongly dependent on TiO_2 crystalline structure. Crystalline structure of commercial TiO_2 P25 nanoparticles is more defined than that of sol-gel generated particles. Large surface area and crystalline structure of TiO_2 P25 nanoparticles lead to better properties. According to the literature [28-32], commercial TiO_2 P25 is known as one of the most effective photocatalysts; however photocatalytic activity of uniform coating of smaller size TiO_2 nanoparticles generated directly on the surface of the fiber via TIP-A sol-gel process approached to its activity.

Change in the color of wine stain was noticed for stained untreated sample exposed to daylight, as well. This indicates that UV light, presented in daylight, is responsible for partial degradation of organic matter in stain. On the basis of the measurements of C^*, discoloration of organic compound (wine stain) was 26.8 %.

Conclusion

Nanocoatings on regenerated cellulose fibers were developed and prepared by two different methods; i.e. using pre-formed commercial TiO_2 P25 nanoparticles and by an in situ approach of preparing nanocoatings using Titanium (IV) isopropoxide precursor via sol-gel process. Homogeneous nanocoatings with uniform TiO_2 nanoparticles distribution were prepared from stable acid TiO_2 P25 nanoparticles dispersion. Significant differences were observed when the sol-gel process for preparation of nanocoatings was applied, especially in reactions arising from presence or absence of water. The results suggest that air moisture during the sol-gel process was sufficient for formation of homogeneous coatings.

Process conditions influenced the formation of TiO_2 coating, which consequently influences the functionality of coated materials. Coatings with superior surface morphology (e.g. large surface area, monodisperse particles) perform better functionality. The highest photocatalytic activity was observed in the case of nanocoatings derived from stable P25Aq-A dispersion. Photocatalytic activity of coatings, generated via TIP-A sol-gel process, under conditions of controlled hydrolysis

approached to that made of TiO_2 P25.

References

1. C. J. Barbe, F. Arendse, P. Comte, M. Jirousek, F. Lenzmann, V. Shklover, and M. Gratzel, *J. Am. Ceram. Soc.*, **80**, 3157 (1997).
2. D. J. Kim, S. H. Hahn, S. H. Oh, and E. J. Kim, *Mat. Lett.*, **57**, 355 (2002).
3. L. Kavan, J. Rathousky, M. Gratzel, V. Shklover, and A. Zukal, *Microporous Mesoporous Mater.*, **44-45**, 653-659 (2001).
4. S. D. Burnside, V. Shklover, C. Barbe, P. Comte, F. Arendse, K. Brooks, and M. Gratzel, *Chem. Mater.*, **10**, 2419 (1998).
5. L. C. Klein, "Sol-gel Optics-processing and Applications", Kluwer Academic Publishers, Boston, 1994.
6. C. J. Brinker, A. J. Hurd, P. R. Schunk, G. C. Frye, and C. S. Ashley, *J. Non-Cryst. Solid.*, **147-148**, 424 (1992).
7. S. Sakka, H. Kozuka, and S. H. Kim, "Ultrastructure Processing of Advanced Ceramics", Wiley, New York, 1988.
8. O. Lev, M. Tsionsky, L. Rabinovich, V. Glezer, S. Sampath, P.I. Ankratov, and J. Gun, *Anal. Chem.*, **67**, 22A (1995).
9. U. Schubert, N. Husing, and A. Lorenz, *Chem. Mater.*, **7**, 2010 (1995).
10. E. J. A. Pope and J. D. Mackenzie, *J. Non-Cryst. Solids*, **87/1-2**, 185 (1986).
11. C. J. Brinker and G. W. Scherer, "Sol-gel Science. Acad. Press", pp.131-136, San Diego, 1990.
12. C. J. Brinker, "Structure of Sol-gel-derived Glasses" In Glass Science and Technology, pp. 169-230, vol. 4A, Boston: Academic Press, Inc., 1990.
13. M. Schraml-Marth, K. L. Walther, A. Wokan, B. E. Handy, and A. Baiker, *J. Non-Cryst. Solids*, **143**, 93 (1992).
14. F. Brunet and B. Cabane, *J. Non-Cryst. Solids*, **163**, 211 (1993).
15. H. F. Ko, C. Sfeirc, and P. Kumta, *Mater. Sci. Eng., C*, **27/3**, 479 (2007).
16. A. Matsuda, Y. Kotani, K. Kogure, M. Tatsumisago, and T. Minami, *J. Am. Ceram. Soc.*, **83/1**, 229 (2000).
17. B. Othani, Y. Ogawa, and S. I. Nishimoto, *J. Phys. Chem. B*, **1001**, 3746 (1997).
18. K. Tanaka, M. F. V. Capule, and T. Hisanaga, *Chem. Phys. Lett.*, **187**, 73 (1991).
19. B. Othani, J. I. Handa, S. I. Nishimoto, and T. Kagiya, *Chem. Phys. Lett.*, **120**, 292 (1985).
20. M. Peplow, *J. Am. Ceram. Soc.*, **87**, 953 (2004).
21. R. Vormberg, *Degussa Sci. Newslett.*, **9**, 21 (2004).
22. J. Andrews, *U. S. Patent*, 6884752, "Photocatalytically-active, Self-cleaning Aqueous Coating Compositions and Methods", New York, 2002.
23. T. Kemmitt, N. I. Al-Sali, M. Wateerland, V. J. Kennedy, and A. Markwitz, *Curr. Appl. Phys.*, **2/4**, 189 (2004).
24. L. Su and Z. Lu, *J. Phys. Chem. Solids*, **59/8**, 1175 (1998).
25. A. Bozzi, T. Yuranova, and J. Kiwi, *J. Photochem. Photobiol. A*, **172/1**, 27 (2005).
26. A. Bozzi, T. Yuranova, I. Guasaquilloa, D. Laubb, and J. Kiwi, *J. Photochem. Photobol. A*, **174/2**, 156 (2005).
27. W. A. Daoud and J. H. Xin, *J. Am. Ceramic Soc.*, **87/5**, 953 (2004).
28. C. Guillard, J. Disdier, J. M. Herrmann, C. Lechaut, T. Chopin, S. Malato, and J. Blanco, *Catal. Today*, **54**, 217 (1999).
29. O. Heintz, D. Robert, and J. V. Weber, *J. Photochem. Photobiol. A*, **135**, 77 (2000).
30. R. R. Bacsa and J. Kiwi, *Appl. Catal., B*, **16**, 19 (1998).
31. R. I. Bickley, T. Gonzalez-Carreno, J. S. Lees, L. Palmisano, and R. J. D. Tilley, *J. Solid State Chem.*, **92**, 178 (1991).
32. A. K. Datye, G. Riegel, J. R. Bolton, M. Huang, and M. R. Prairie, *J. Solid State Chem.*, **115**, 236 (1995).
33. J. Winkler, "Titanium Dioxide", pp.80-101 European Coatings Literature, Vincentz, 2003.
34. D. N. Furlong and G. D. J. Parfitt, *J. Colloid Interface Sci.*, **69**, 409 (1979).
35. A. Bonincontro, E. Spigone, M. Ruiz-Pena, C. Letizia, and C. La Mesa, *J. Colloid Interface Sci.*, **304**, 342 (2006).
36. C. Letizia, P. Andreozzi, A. Scipioni, C. La Mesa, A. Bonincontro, and E. Spigone, *J. Phys. Chem. B*, **111**, 898 (2007).
37. A. W. Adamson, "Physical Chemistry of Surfaces", Vth Edition, Ch. V, p. 218, Willey, New York, 1991.
38. A. Bonincontro, C. La, Mesa, C. Proietti, and G. Risuleo, *Biomacromolecules*, **8**, 1824 (2007).
39. http://www.arso.gov.si, Accessed 18 Nov. 2008.
40. V. Golob and D. Golob, Teorija Barvne Metrike. V: Interdisciplinarnost Barve, Part 1, 2001.
41. K. McLaren, "Colour Physics for Industry", Edited by McDonald R., Ch. VI, Society of Dyeres and Colourist, England, 1987.
42. www.malvern.com, Accessed 20 Feb. 2009.
43. X. Chen, H. Cheng, and J. Ma, *Powder Tech.*, **99**, 171 (1998).
44. D. Regitsky, Project "Use of Emulsion Polymerization to Prepare Inorganic/Polymer Nanocomposites for Application in Creating Lotus Effect Surfaces" (2005); http://www.prc.gatech.edu/academics/pre-college/hs-projects/fall2005/DrewRegitskyReport.pdf Accessed 28 Nov. 2008.
45. S. Sakka, *J. Sol-gel Sci. Tech.*, **3/2**, 69 (1994).
46. B. Tomšič, B. Simončič, J. Vince, B. Orel, A. Vilnik, M. Fir, A. Šurca Vuk, and V. Jovanovski, *Tekstilec*, **50/1-3**, 3 (2007).
47. G. D. Parfitt, "Surface Chemistry of Oxides", Tioxide International Ltd., Billingham, Cleveland, UK, Pure & Appl. Chem., 48, pp.415-418. Pergamon Press, Printed in Great Britain, 1976.
48. M. Primet, P. Pichat, and M. V. Mathieu, *J. Phys. Chem.*, **75**, 1216 (1971).
49. P. A. Connor, K. D. Dobson, and A. J. McQuillan, *Langmuir*, **15**, 2402 (1999).

50. B. Erdem, R. A. Hunsicker, G. W. Simmons, E. D. Sudol, V. L. Dimonie, and M. S. El-Aasser, *Langmuir*, **17**, 2664 (2001).
51. F. Sayilkan, H. Sayilkan, S. Erdemoglu, S. Sener, and M. Akarsu, *Turkish J. Chem.*, **28**, 27 (2004).
52. H. Nur, *Mat. Sci. and Eng. B,* **133**, 49 (2006).
53. S. J. Lee, S. W. Han, M. Yoon, and K. Kim, *Vib. Spectrosc.*, **24**, 265 (2000).
54. M. N. Belgacem and A. Gandini, *Polímeros*, **15/2**, 114 (2005); http://www.scielo.br/scielo, Accessed 24 Oct. 2008.
55. D. J. Kim, S. H. Hahn, S. H. Oh, Accessed E. J. Kim, *Mat. Lett.*, **57**, 355 (2002).